

Journal of Materials Chemistry C

Accepted Manuscript



This is an *Accepted Manuscript*, which has been through the Royal Society of Chemistry peer review process and has been accepted for publication.

Accepted Manuscripts are published online shortly after acceptance, before technical editing, formatting and proof reading. Using this free service, authors can make their results available to the community, in citable form, before we publish the edited article. We will replace this *Accepted Manuscript* with the edited and formatted *Advance Article* as soon as it is available.

You can find more information about *Accepted Manuscripts* in the [Information for Authors](#).

Please note that technical editing may introduce minor changes to the text and/or graphics, which may alter content. The journal's standard [Terms & Conditions](#) and the [Ethical guidelines](#) still apply. In no event shall the Royal Society of Chemistry be held responsible for any errors or omissions in this *Accepted Manuscript* or any consequences arising from the use of any information it contains.

Performance improvement of GaN-based light-emitting diodes grown on Si (111) substrates by controlling the reactor pressure of GaN nucleation layers

Yunhao Lin,^a Shizhong Zhou,^a Wenliang Wang,^a Weijia Yang,^a Huirong Qian,^a Haiyan Wang,^a Zhiting Lin,^a Zuolian Liu^a, Yunnong Zhu^a and Guoqiang Li^{*ab}

^a State Key Laboratory of Luminescent Materials and Devices, South China University of Technology, Guangzhou 510641, China

^b Department of Electronic Materials, South China University of Technology, Guangzhou 510641, China. E-mail: msgli@scut.edu.cn

Abstract

GaN-based light-emitting diodes (LEDs) with various reactor pressures for GaN nucleation layers (NLs) have been grown on Si (111) substrates by metal-organic chemical vapor deposition. The influence of reactor pressure for GaN NLs on the properties of GaN-based LEDs grown on Si (111) substrates is investigated in detail. It is revealed that crack-free GaN films are grown on the Si (111) substrate. As the reactor pressure for GaN NLs increases from 200 to 600 Torr, the full width at half maximum values of the X-ray diffraction rocking curves for the GaN (0002) and (10-12) planes decrease from 480 to 351 arcsec, and 868 to 445 arcsec, respectively, and therefore the threading dislocation density is greatly reduced, which is confirmed by the cross-sectional transmission electron microscopy measurement. Subsequently, the relationship between the bending and annihilation for dislocations and the modes for GaN NL are elucidated. Meanwhile, the effect of reactor pressure for GaN NL on the mode of GaN NL is also systematically studied. Furthermore, the light output power of GaN-based LEDs with GaN NLs grown at reactor pressure of 500 Torr is greatly improved by 73.66% in comparison with that of GaN-based LEDs with GaN NLs grown at reactor pressure of 200 Torr. This work provides a new approach for achieving highly-efficient GaN-based LEDs on Si (111) substrates.

1. Introduction

To date, illumination devices fabricated with GaN and its related III-nitrides, like lighting

emitting diodes (LEDs) and laser diodes (LDs), have been commercialized.¹⁻³ In general, GaN films are grown on sapphire and SiC substrates.^{1,2} The relevant devices grown on these foreign substrates, however, face difficulties in wider promotion and application due to their high cost. Recently, GaN-based LEDs grown on Si substrates by metal-organic chemical vapor deposition (MOCVD) have attracted enormous attention thanks to the advantages of Si, such as low cost, large size, *etc.* However, the epitaxial growth of GaN films on Si substrates still has at least three challenges by now.³⁻⁶ First, there are serious chemical reactions existing between Ga and Si at elevated temperatures, which might directly hamper the growth of GaN on Si. Second, the large thermal coefficient mismatch (54%) between GaN and Si will induce massive tensile stresses. As a result, cracks are generated on the surface of GaN. Third, high density dislocations, which results from the large lattice mismatch (16.9%), can act as non-radiative recombination centers to diminish LEDs efficiency.^{7,8}

So far, many approaches have been deployed to solve these problems. It is reported that the chemical reactions between Ga and Si can be solved by the insertion of AlN⁹⁻¹¹ Al₂O₃,¹² or ZrB₂¹³ buffer layer, to isolate Ga from Si. Solutions, such as selective epitaxy to isolate the growth area,¹⁴⁻¹⁶ Al_xGa_{1-x}N buffer layer,¹⁷⁻²⁰ AlN interlayer,²¹⁻²⁵ AlGaN interlayer,²⁶ and AlN/GaN superlattice interlayer,^{27,28} have been deployed to prevent cracks induced by tensile thermal stress and to suppress threading dislocations. Through these measures, the GaN-based LED devices on Si substrates have been fabricated successfully. Dadgar *et al.* achieved 5.4 μm-thick crack-free GaN-based LED structures on Si (111) substrates using the low temperature AlN interlayers to counterbalance the tensile thermal stress during the cooling process. The FWHM for the GaN (0002) of 380 arcsec could be obtained,²⁴ but the light output power for GaN-based LEDs on Si substrates with 360 μm in diameter is only 0.152 mW at 20 mA.²¹ Zhu *et al.* used step graded AlGaN buffers and Si_xN_y interlayer to improve the performance of GaN-based LEDs on Si substrates. The cracks and threading dislocations are suppressed by the step graded AlGaN buffers and Si_xN_y interlayer, and density of threading dislocations is further decreased to 6.2×10⁸ cm⁻².³ Meanwhile, the light output power for 500×500 μm² LED chips on Si substrates is 0.5 mW at 20 mA.²⁹ In this regard, most studies for LEDs on Si substrates focus on the structures of hetero-buffer and interlayers, and the effect of growth conditions for GaN itself on GaN-based LEDs on Si substrates has been rarely reported.

Herein, we report on the growth of highly-efficient GaN-based LED wafers on Si substrates by MOCVD with three GaN nucleation layers (NLs). The effect of reactor pressure for GaN NLs on the stress and crystalline quality of GaN films is investigated in detail and the underlying mechanisms are proposed. Furthermore, the optoelectronic properties of crack-free GaN-based LEDs on Si (111) substrates with various reactor pressures for GaN NLs are detailed in this work. An effective approach for obtaining highly-efficient LEDs on Si (111) substrates is hence presented.

2. Experimental Procedure

All the samples were grown by Veeco K465i MOCVD on 2-inch Si (111) substrates. Trimethyl gallium(TMGa), trimethyl aluminium(TMAI), trimethyl indium (TMIn) and ammonia were used as precursors for Ga, Al, In and N, respectively. Silane (SiH_4) and cyclopentadienyl magnesium (Cp2Mg) were used as the sources of the n-type and p-type dopants, respectively. N_2 was used as carrier gases. A 80 nm-thick AlN buffer layer was deposited directly on the substrates, followed by a 650 nm-thick AlGaIn buffer layer. Then, three AlN interlayers with GaN NLs and u-GaN layer/n-GaN layer (Si-doping concentration is $4.5 \times 10^{18} \text{ cm}^{-3}$) were deposited on the AlGaIn buffer. Furthermore, the as-grown LED structures included five periods InGaIn (3 nm) /GaIn (12 nm) MQWs, 20 nm-thick p-AlGaIn layer and 150 nm-thick p-GaN layers were grown on the upper n-GaN layer. The whole structure was shown in Fig. 1 a. The GaN NLs were grown at 200, 350, 500, and 600 Torr with the identical LED structure mentioned, and these samples were denoted as Sample A, B, C and D, respectively. The GaN NLs grown at 200, 350, 500 and 600 Torr were prepared on AlN interlayer-1 to study the growth modes of the GaN NL on different reactor pressures, the structures of GaN NL are shown in Fig. 1 b. The growth temperatures of GaN NLs, u-GaN, n-GaN were all 1030 °C, and the growth reactor pressure of both u-GaN and n-GaN were 200 Torr.

Finally, the as-grown LED wafers were made into chips with a size of $500 \times 500 \mu\text{m}^2$ with the standard processes.¹

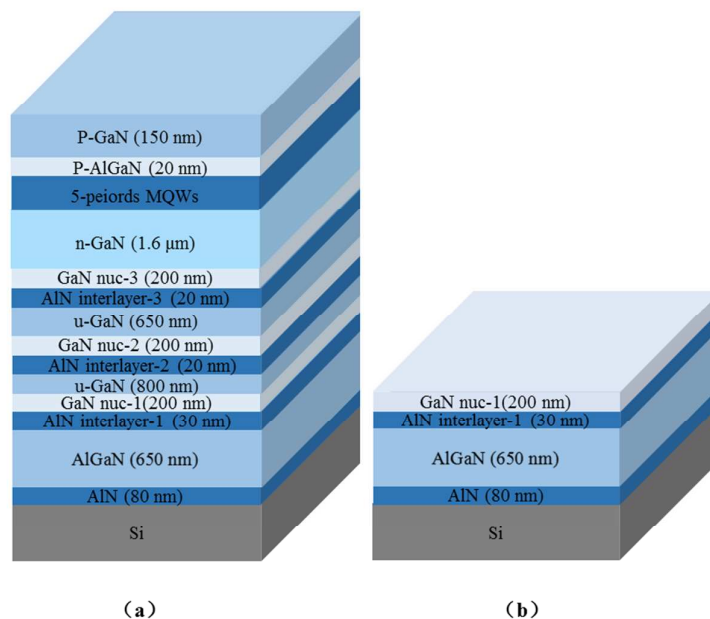


Fig. 1. (a) The structure of Sample A, B, and C, and (b) the structure of GaN NL on the AlN interlayer-1.

The crystalline quality of GaN was characterized by high-resolution X-ray diffraction (HRXRD, Bruke D8 X-ray diffractometer with $\text{CuK}\alpha 1$ X-ray source, $\lambda=1.5406 \text{ \AA}$) and high-resolution transmission electron microscopy (HRTEM, JEOL3000F). The surface morphologies were studied by atomic force microscopy (AFM, Bruker Dimension Edge) and optical microscopy (OLYMPUS, BX51M). The stresses were probed by the micro-Raman spectroscopy (Renishaw inVia Raman spectrometer with a 532 nm laser as the excitation source). The optical properties were measured by a 405 nm laser (Y-Wafer GS4-GaN-R-405) exciting source with an output power of 20 mW at room temperature (RT). The optoelectronic properties of the LED chips were investigated by GAMMA Scientific GS-1190 RadoMA-Lite KEITHLEY 2400 system.

3. Results and discussion

Fig. 2 reveals the smooth surfaces of Sample A, B, C and D. It can be noted that there are no cracks existing in Sample A, B and C. However, Sample D with the GaN NLs at 600 Torr has 1.23 mm^{-2} density of cracks. The crack-free GaN films of Sample A, B, C can be ascribed to the reduction of residual tensile stress, which is known as the origin of the cracks. In general, this residual tensile stress derives mainly from the thermal mismatch during the cooling process.³¹ In

addition, the impurities such Si, Mg and O can also induce the tensile stress during the growth of GaN layer.³¹ Furthermore, the coalescence of the GaN islands make significant contribution to the formation of tensile stress in GaN layer.³² Nevertheless, this tensile stress can be compensated by the compressive stress that results from the AlN interlayers,²¹⁻²⁵ and AlN/AlGaIn buffer layer.¹⁷⁻²⁰

The Raman scattering is used to analysis the residual stress of GaN on Si substrates. The Raman spectra of Samples A, B, C and D measured at room temperature are presented in Fig. 3a. The phonon peak at around 520 cm⁻¹ is from the Si(111) substrate, and the phonon peak locates at the right of the Si phonon peak is GaN E₂ (high) peak.³³ Fig. 3b indicates that the GaN E₂(high) photon peak positions of Samples A, B, C and D are 567.6, 566.1, 564.8 and 566.2 cm⁻¹, respectively. The 567.5 cm⁻¹ known as the stress-free GaN E₂(high) phonon peak is used as a reference peak to calculate the stress. The definite stress of GaN can be evaluated by the following equation³³⁻³⁵

$$\Delta \omega = 4.3\sigma_{xx}cm^{-1}GPa^{-1}$$

In this equation, $\Delta\omega$ is the E₂ (high) phonon peak shift, and σ_{xx} represents the biaxial stress of the GaN. According to this equation, the residual stresses of Samples A, B, C and D are calculated to be 0.23, -0.326, -0.628 and -0.302 GPa, respectively. It can be noticed that Sample A is under compressive stress, which confirms the stress compensation by the AlN/AlGaIn buffer and AlN interlayers. However, in Samples B and C, it turns into tensile stress and the tensile stress rises as the increase in reactor pressure from 200 to 500 Torr. We deduce that the stress transition and the increase of the residual tensile stress for Samples A, B and C originate from the coalescence of GaN islands, which induces the tensile stress during the growth process. Regarding to Sample D, when the reactor pressure for GaN NLs reaches 600 Torr, the residual tensile stress exceeds the critical value. As a consequence, the residual tensile stress is released slowly by generating cracks during the cooling process.³³ Therefore, the residual tensile stress in Sample D is lower than that in Samples B and C.

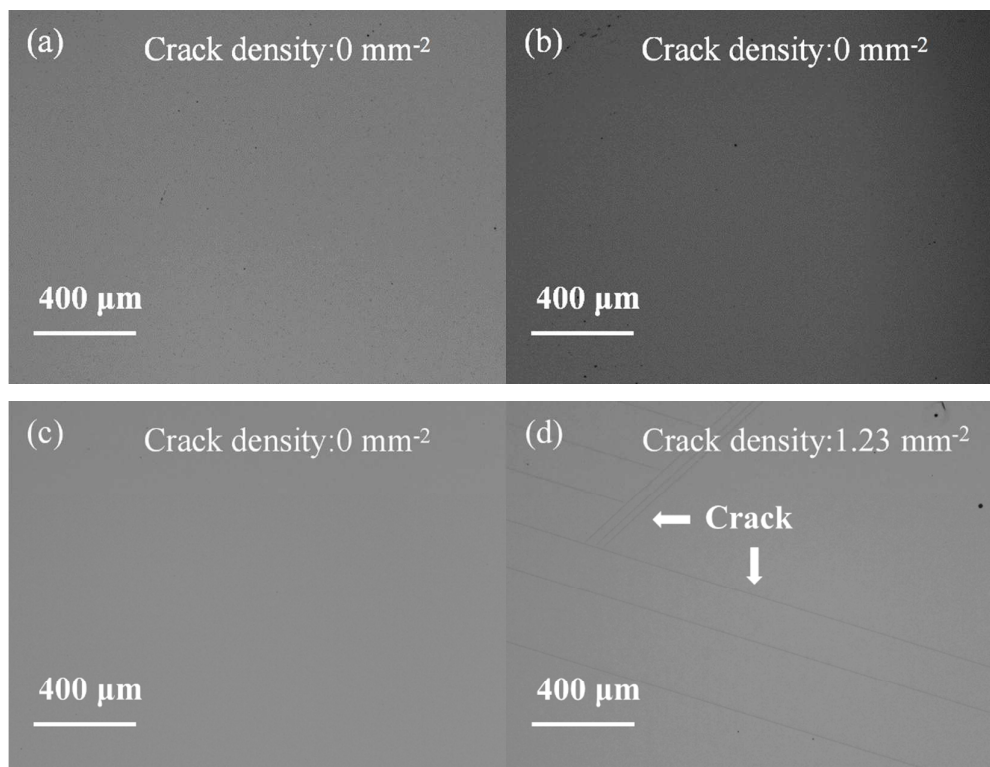


Fig. 2. Optical microscopic images of Sample (a) A, (b) B, (c) C and (d) D.

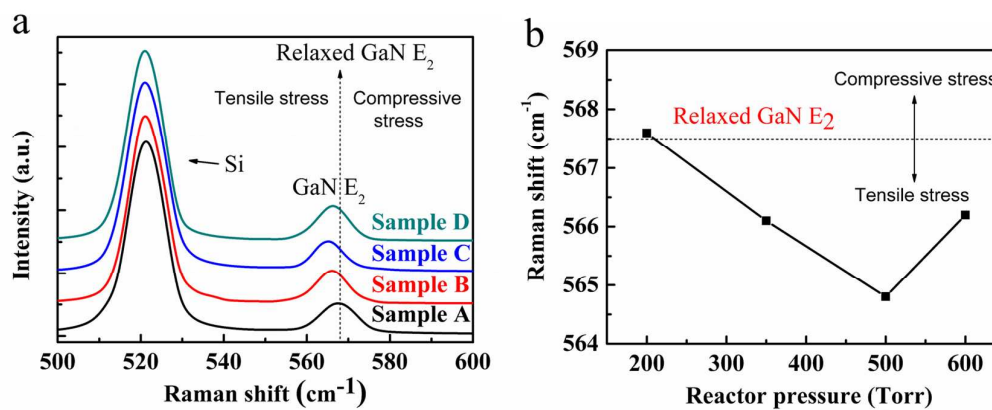


Fig. 3. (a) Raman spectra and (b) dependence of GaN E₂ Raman shift on the reactor pressure of GaN NLs for Sample A, B, C and D.

Fig. 4a shows the full width at half maximum (FWHM) values of the X-ray diffraction rocking curves (XRCs) for GaN (0002) and (10-12) planes of Sample A, B, C and D. The FWHMs of GaN (0002) and (10-12) planes decrease from 480 to 351 arcsec and 868 to 445 arcsec, respectively, as the reactor pressure for GaN NLs increases from 200 to 600 Torr. The typical XRCs of GaN (0002) and (10-12) for crack-free Sample C are displayed in Figs. 4b and c. The FWHMs of GaN (0002)

and (10-12) planes for Sample C are 363 and 467 arcsec, respectively. It is apparent that the GaN film with GaN NLs grown at high reactor pressure exhibits much better crystalline quality than that with GaN NLs grown at low reactor pressure. As we know, the (0002) FWHM is related to the dislocations in screw component, while the (10-12) FWHM is related to the amount of edge dislocations and mixed dislocations.^{36,37} The dislocation density in GaN layer can be evaluated by FWHM using the following equation:³⁶

$$D_{dis} = \beta^2 / 9b^2 \quad (1)$$

In this equation, D_{dis} represents the dislocation density, β is the FWHM value of XRC, and b is the length of the Burger vector of the corresponding dislocation. Based on this equation, the estimated screw (edge and mixed) dislocation densities of Sample A, B are 1.75 (3.45) and 1.34 (1.93) times as compared with that of Sample C. Hence, we believe that there is better inhibition for dislocations in the GaN films with GaN NLs grown at higher reactor pressure as compared with the GaN film with lower reactor pressure for GaN NLs.

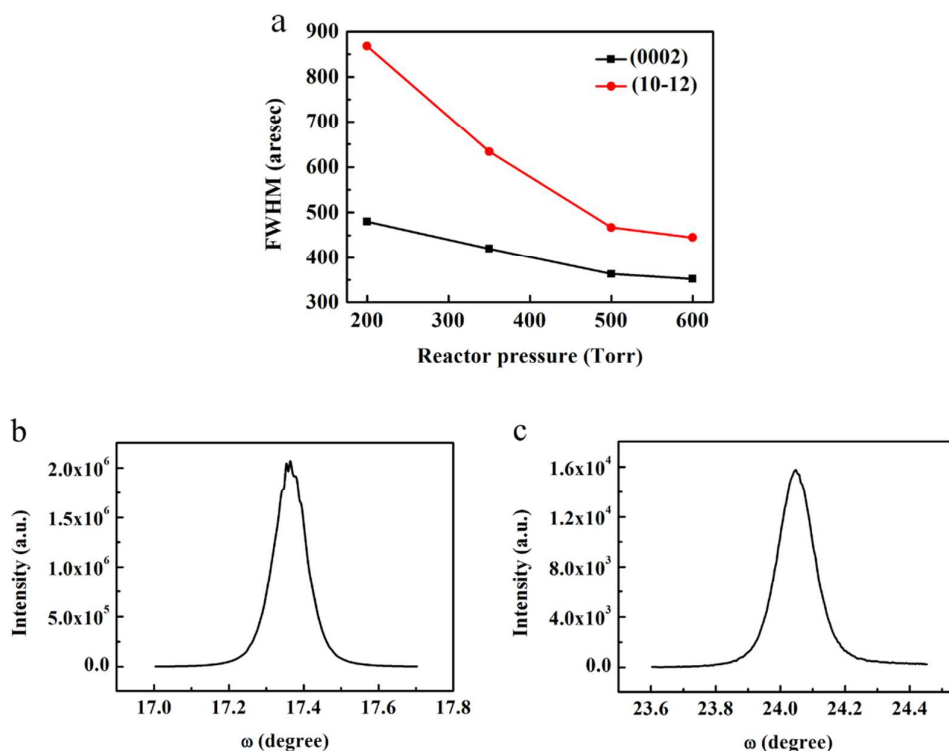
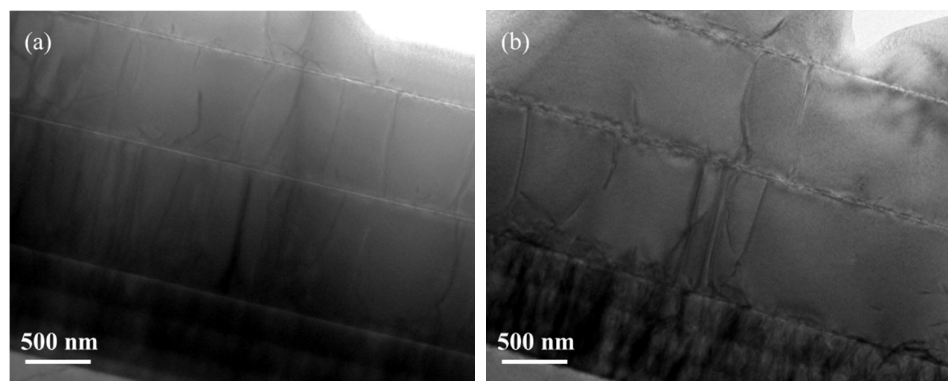


Fig. 4. (a) Dependence of FWHM on the reactor pressure of GaN NLs for Sample A, B, C and D. The typical XRCs for (b) GaN (0002) and (c) GaN (10-12) of Sample C.

TEM is employed to understand the above results from the XRC analysis. Figs. 5a and b show the cross-sectional bright field-TEM (BF-TEM) image of Sample A with GaN NLs at 200 Torr and Sample C with 500 Torr. It is obvious that the number of dislocations in the upper GaN layers is much less in both Sample A and Sample C. It is confirmed that the threading dislocations are blocked by AlN interlayers.²³⁻²⁷ However, there is a significant difference in the dislocation density between Sample A and Sample C. Detailed study of dislocations has been performed in Figs. 5c and d. It could be found that the majority of dislocations from the interface of AlN interlayer-1 and GaN propagates into the upper GaN layer in Sample A, as shown in Fig. 5c. This phenomenon is in striking contrast to that in Sample C. From Fig. 5d, one can notice some bending and annihilation of dislocations above the AlN interlayers. These bending and annihilation of dislocations, which occur above each AlN interlayers, eventually reduce the density of threading dislocations. These results are well consistent with the XRC analysis. We attribute the reduction of threading dislocation for Sample C to two aspects. One is the obstruction of the AlN interlayers for the dislocations, and the other is the bending and annihilation of the dislocations which originate from the GaN NLs at high reactor pressure. However, as for Sample A, the reduction in threading dislocation density just result from the obstruction of the AlN interlayers for dislocations. Therefore, the dislocation density for Sample A is much higher than Sample C.



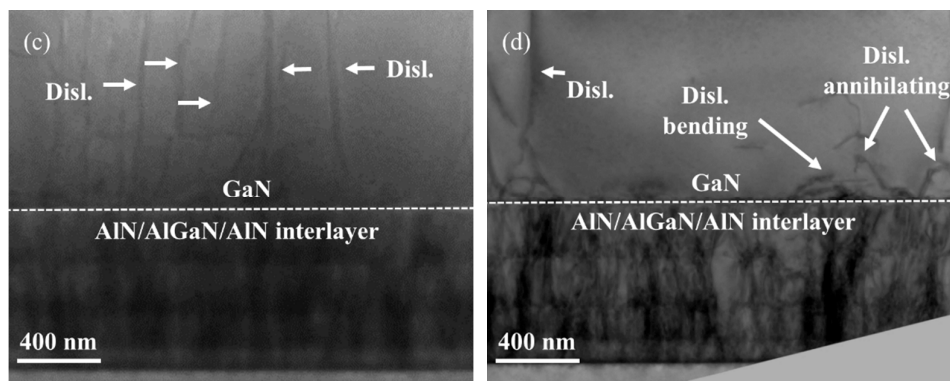


Fig. 5. Cross-sectional BF-TEM images of (a) Sample A and (b) Sample C, and the detailed cross-sectional BF-TEM images of GaN layer on the AlN interlayer-1 for (c) Sample A and Sample C.

Fig. 6 shows the reactor pressure dependence of the root mean square (RMS) roughness of as-grown GaN NL by AFM. It can be noted that the RMS roughness increases monotonously as the reactor pressure increases. The RMS roughness value of the GaN NL grown at 500 Torr is 8.7 nm, which shows a mosaic of faceted grains and the boundaries of the GaN grains. On the contrary, the surface of GaN NL grown at 200 Torr is much smoother with a RMS roughness of 2.5 nm, and the boundaries of the GaN grains are obscure. The larger RMS roughness of the GaN nucleation layer grown on higher reactor pressure can be attributed to the suppression of lateral growth and prevention for the coalescence of GaN islands.^{30,41} We find that these difference conditions of coalescence may be correlated to the different growth modes for GaN NL. The rough GaN NL surface grown at 500 Torr indicates that the growth mode of GaN NL is three dimension growth mode, while the GaN NL grown at 200 Torr shows the almost fully coalesced surface which reveals the two dimension growth mode. The growth modes of GaN NL are consistent with the stress analysis mentioned above. The GaN NL with rougher surface due to the higher reactor pressure needs more time to coalesce,³⁰ leading to suffering stronger tensile stress in GaN layer. Therefore, the cracks generate more easily for GaN NLs grown at higher reactor pressure.

As regarding to the dislocations, it has been reported that, during the low reactor pressure growth, the beginning of the growth of GaN NL leads to the formation of GaN grains with inclined vertical facets of $\{10-10\}$ or $\{11-20\}$. In this case, the dislocations stretch along the

$\langle 0001 \rangle$ -axis and penetrate to the GaN surfaces. Nevertheless, the GaN NL grown at high reactor pressure tends to the formation of GaN grains slant side facets, either $\{1-101\}$ or $\{11-22\}$, allows dislocations to extend along the growth orientation of GaN grain facets, and then during the coalescence process of GaN grains, bends of the dislocations occur.³⁹⁻⁴¹ Based on the characterizations, it can be deduced that the dislocation evolutions in this case are similar to the situations mentioned above. The growth process for GaN films with the GaN NL grown at 200 Torr is illustrated in Fig. 7a. In this process, the GaN NL tends to the two dimension growth mode, which facilitates the GaN grains to coalesce rapidly. Consequently, the flat surface morphology of GaN NL is obtained, as shown in Fig. 6. In this mode, the majority of dislocations penetrates into GaN surface and evaluates into the threading dislocations as the growth of the GaN layer. The growth process for GaN films with the GaN NL grown at 500 Torr is illustrated in Fig. 7a. The growth mode for GaN NL grown at 500 Torr is three dimensional growth mode. Subsequently, in the processes of u-GaN/n-GaN epitaxy, the dislocations propagate along the flank epitaxial surface as the lateral growth rate is increased by changing the growth conditions. Finally, the dislocations bend and annihilate, and are terminated above the AlN interlayers.

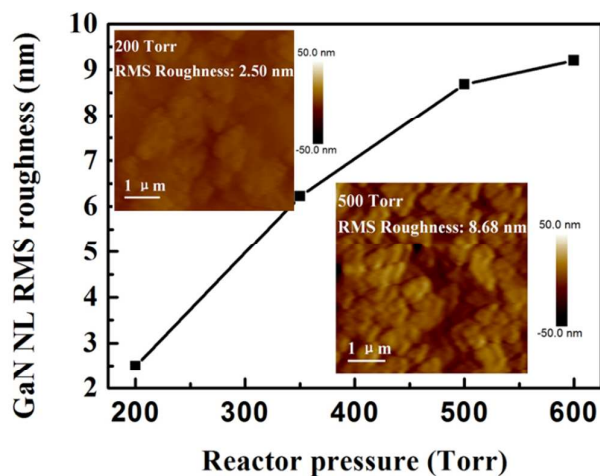


Fig. 6. Surface RMS roughness of GaN NL as a function of reactor pressure. The insets are the surface morphology of GaN NL grown at 200 and 500 Torr.

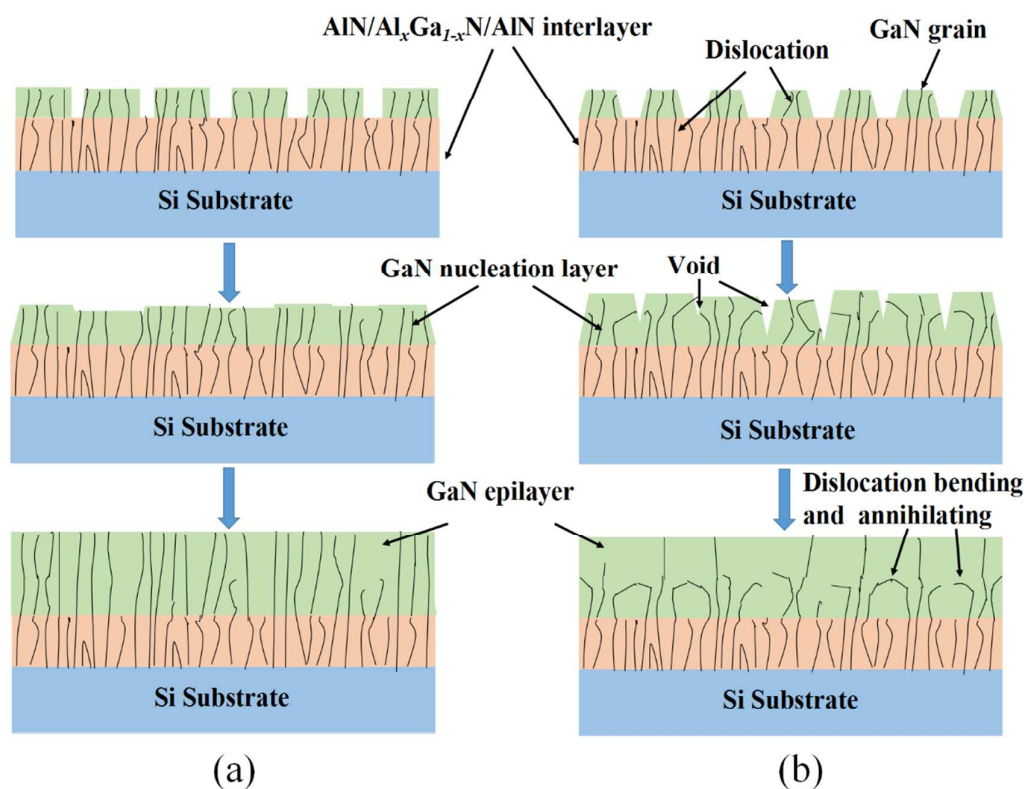


Fig. 7. The schematic drawings of the propagation for dislocations with GaN NL grown on (a) 200 and (b) 500 Torr

The influence of reactor pressures for GaN NLs on the optoelectronic properties of as-grown crack-free LED structures is studied by photoluminescence (PL) at room temperature, as shown in Fig. 8. It can be noted that the highest intensity of PL peak is obtained from Sample C, and the intensity of PL peak for Sample B is better than that for Sample A. Meanwhile, the FWHMs of PL peak of Sample A, B and C are 22.7, 21.8, and 20.5 nm, respectively. Sample C is of the highest intensity and smallest FWHM for PL peak, which indicates the highest quality MQWs on Si substrates. We attribute the results to the reduction of threading dislocations, which act as non-radiative recombination centers or as associated pits for absence of the QW on the pit facets and is detrimental to the radiative recombination.^{7,8,38} This result promotes the radiative recombination of holes and electrons and eventually enhances the internal quantum efficiency (IQE) of MQWs. Therefore, the reduction of threading dislocations by growing GaN NLs at high pressure can improve the optoelectronic properties of GaN-based LEDs on Si substrates effectively, especially the IQE of MQWs.

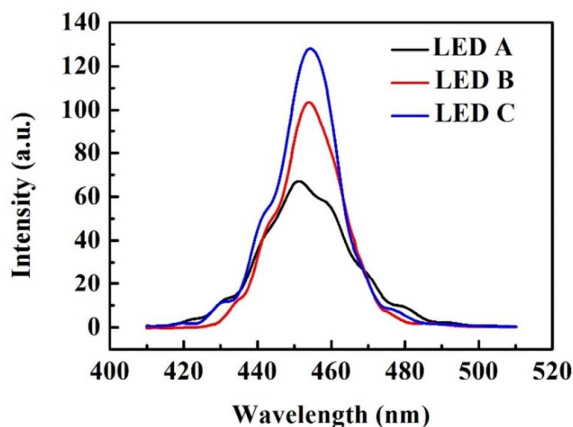
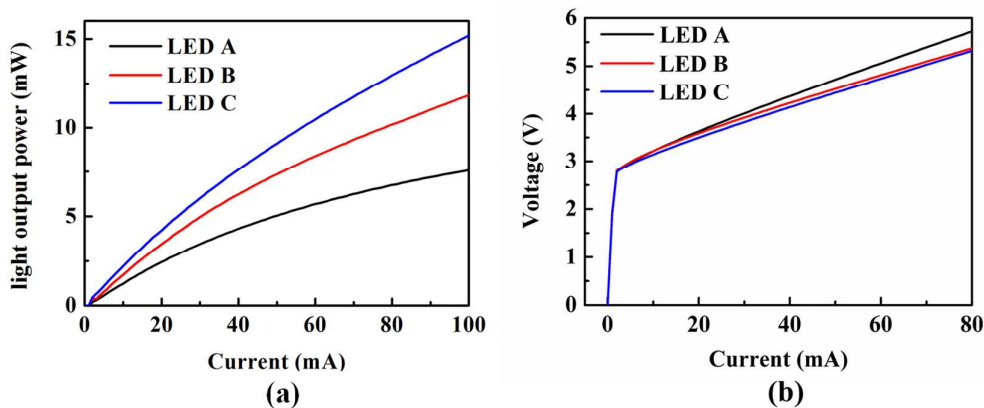


Fig. 8. PL spectrums of LED-A, B, C at room temperature with 405 nm laser as the excitation source

Light output power (L)-current (I) and the current-voltage (V) curves for LED chips from Samples A, B and C with the size of $500 \times 500 \mu\text{m}^2$ are shown in Fig. 9. It can be easily noted that the light output power for these three samples increases monotonously with the increase in current from Fig. 8. Furthermore, it shows that at a current injection of 20 mA, the forward bias voltage for chips of Sample A, B and C is 3.63, 3.58 and 3.47 V, respectively, and the light output power of chips for Sample A, B and C is 2.43, 3.44 and 4.22 mW, respectively. Therefore, the results confirm the best optoelectronic properties of chips from Sample C, and are well consistent with the measurement of PL. In this regard, the achievement of improvement for LED performance can be attributed to the promotion of IQE for MQWs, which results from the reduction of threading dislocations by controlling the reactor pressure of GaN NLs.





(c)

Fig. 9. (a) Light output power v.s. current, and (b) voltage v.s. current curves of LED chips from Samples A, B and C, and (c) the light emission image of LED chip from Sample C

Conclusion

Crack-free high-quality GaN-based LEDs grown on Si (111) substrates can be achieved by growing GaN NLs under 500 Torr. The influence of reactor pressure for GaN NLs on the properties of crack-free GaN-based LEDs grown on Si (111) substrates is investigated in detail. It is demonstrated that the growth mode of the GaN NLs changed from two dimension mode to three dimension mode as the reactor pressure increases from 200 to 500 Torr, In the three dimension growth mode, the dislocations bend and annihilate during the process of coalescence for GaN grains. These bending and annihilation of dislocations suppress the propagation of dislocations to the upper GaN and MQWs effectively, which results in the improvement in the IQE of MQWs, and eventually improves the performance of LED chips on Si substrates.

References

1. W. L. Wang, Y. H. Lin, W. J. Yang, Z. L. Liu, S. Z. Zhou, H. R. Qian, F. L. Gao, L. Wen and G. Q. Li, *J. Mater. Chem. C*, 2014, **2**, 4112-4116.
2. A. Y. Polyakov, S. J. Pearton, P. Frenzer, F. Ren, L. Liu and J. Kim. *J. Mater. Chem. C*, 2013, **1**, 877-887.
3. D. D. Zhu, D. J. Wallis and C. J. Humphreys, *Rep. Prog. Phys.*, 2013, **76**, 106501.
4. A. Krost and A. Dadgar, *Mater. Sci. Eng., B*, 2002, **93**, 77-84.

5. H. Ishikawa, K. Yamamoto, T. Egawa, T. Soga, T. Jimbo and M. Umeno, *J. Cryst. Growth*, 1998, **189/190**, 178-182.
6. T. Y. Wang, S. L. Ou, R. H. Horng and D. X. Wu, *CrystEngComm.*, 2014, **16**, 5724-5731.
7. S. Suihkonen, M. Ali, P. T. Torma, S. Sintonen, O. Svensk, M. Sopanen, H. Lipsanen, V. N. Nevedomsky and N. A. Bert, *Jpn. J. Appl. Phys.*, 2013, **52**, 01AF01.
8. J. Hsu, M. J. Manfra, R. J. Molnar, B. Heying and J. S. Speck, *Appl. Phys. Lett.*, 2002, **81**, 79-81.
9. W. J. Luo, X. L. Wang, L. C. Guo, H. L. Xiao, C. M. Wang, J. X. Ran, J. P. Li and J. M. Li, *Microelectron. J.*, 2008, **39**, 1710-1713.
10. S. Zamir, B. Meyler, E. Zolotoyabko and J. Salzman, *J. Cryst. Growth*, 2000, **218**, 181-190.
11. H. Marchand, L. Zhao, N. Zhang, B. Moran, R. Coffie, U. K. Mishra, J. S. Speck, S. P. DenBaars and J. A. Freitas, *J. Appl. Phys.*, 2001, **89**, 7846-7851.
12. W. E. Fenwick, N. Li, T. Xu, A. Melton, S. Wang, H. Yu, C. Summers, M. Jamil and I. T. Ferguson, *J. Cryst. Growth*, 2009, **311**, 4306-4310.
13. A. H. Blake, D. Caselli, C. Durot, J. Mueller, E. Parra, J. Gilgen, A. Boley, D. J. Smith, I. S. T. Tsong, J. C. Roberts, E. Piner, K. Linthicum, Jr. J. W. Cook, D. D. Koleske, M. H. Crawford and A. J. Fischer, *J. Appl. Phys.*, 2012, **111**, 033107.
14. K. M. Lau, Z. Baoshun, L. Hu, W. Yong, F. Zhihong and W. N. Kar, *J. Cryst. Growth*, 2007, **298**, 725-730.
15. K. M. Lau, K. M. Wong, X. Zou and P. Chen, *Opt. Express.*, 2011, **19**, A956-A961.
16. J. L. Liu, J. L. Zhang, Q. H. Mao, X. M. Wu and F. Y. Jiang, *CrystEngComm.*, 2013, **15**, 3372-3376.
17. R. F. Xiang, Y. Fang, J. N. Dai, L. Zhang, C. Y. Su, Z. H. Wu, C. H. Yu, H. Xiong, C. Q. Chen and Y. Hao, *J. Alloys. Compd.*, 2011, **509**, 2227-2231.
18. M. H. Kim, Y. G. Do, H. C. Kang, D. Y. Noh and S. J. Park, *Appl. Phys. Lett.*, 2001, **79**, 2713-2715.
19. J. Lee, Y. Tak, J. Kim, H. Hong, S. Chae, B. Min, H. Jeong, J. Yoo, J. Kim and Y. Park, *J. Cryst. Growth*, 2011, **315**, 263-266.
20. E. Arslan, M. K. Ozturk, A. Teke, S. Ozcelik and E. Ozbay, *J Phys D Appl Phys*, 2008, **41**, 155317.

21. A. Dadgar, M. Poschenrieder, O. Contreras, J. Christen, K. Fehse, J. Blasing, A. Diez, F. Schulze, T. Riemann, F. A. Ponce and A. Krost, *Phys. Status Solidi A*, 2002, **192**, 308-313.
22. P. Drechsel and H. Riechert, *J. Cryst. Growth*, 2011, **315**, 211-215.
23. J. Blasing, A. Reiher, A. Dadgar, A. Diez and A. Krost, *Appl. Phys. Lett.*, 2002, **81**, 2722-2724.
24. A. Dadgar, C. Hums, A. Diez, J. Blasing and A. Krost, *J. Cryst. Growth*, 2006, **297**, 279-282.
25. T. Egawa and B. A. Shuhaimi, *J. Phys. D: Appl. Phys.*, 2010, **43**, 35400835.
26. S. Fritze, P. Drechsel, P. Stauss, P. Rode, T. Markurt, T. Schulz, M. Albrecht, J. Blasing, A. Dadgar and A. Krost, *J. Appl. Phys.*, 2012, **111**, 124505.
27. J. Ma, X. L. Zhu, K. M. Wong, X. B. Zou and K. M. Lau, *J. Cryst. Growth*, 2013, **370**, 265-268.
28. E. Feltn, B. Beaumont, M. Laugt, P. de Mierry, P. Vennegues, H. Lahreche, M. Leroux and P. Gibart, *Appl. Phys. Lett.*, 2001, **79**, 3230-3232.
29. D. D. Zhu, C. McAleese, M. Haeberlen, C. Salcianu, T. Thrush, M. Kappers, A. Phillips, P. Lane, M. Kane, D. Wallis, T. Martin, M. Astles, N. Hylton, P. Dawson and C. Humphreys, *J. Appl. Phys.*, 2011, **109**, 014502.
30. S. Figge, T. Bottcher, S. Einfeldt and D. Hommel, *J. Cryst. Growth*, 2000, **221**, 262-266.
31. Y. Fu, D. A. Gulino and R. Higgins, *J. Vac. Sci. Technol. A*, 2000, **18**, 965-967.
32. C. Kai, M. Leys, S. Degroote, B. Van Daele, S. Boeykens, J. Derluyn, M. Germain, G. Van Tendeloo, J. Engelen and G. Borghs, *J. Electron. Mater.*, 2006, **35**, 592-598.
33. S. Tripathy, S. J. Chua, P. Chen and Z. L. Miao, *J. Appl. Phys.*, 2003, **93**, 789.
34. D. Wang, S. Jia, K. J. Chen, K. M. Lau, Y. Dikme, P. van Gemmer, Y. C. Lin, H. Kalisch, R. H. Jansen and M. Heuken, *J. Appl. Phys.*, 2005, **97**, 056103.
35. W. L. Wang, W. J. Yang, Z. L. Liu, Y. H. Lin, S. Z. Zhou, H. R. Qiang, F. L. Gao, *J. Mater. Sci.*, 2014, **49**, 3511-3518.
36. S. T. Li, F. Y. Jiang, G. H. Fan, W. Q. Fang and L. Wang, *Phys. B*, 2007, **391**, 169-173.
37. W. L. Wang, H. Yang and G. Q. Li, *J. Mater. Chem. C*, 2013, **1**, 4070-4077.
38. L. Y. Jung, T. T. Yuan, Y. C. Hung, C. L. Yang, T. T. Han, H. C. Chang, C. T. You, H. C. Hsiang and L. W. Chau, *Opt. Express*, 2010, **18**, 2729-2742.

39. H. J. Scheel, *J. Cryst. Growth*, 2000, **211**, 1-12.
40. K. Hiramatsu, K. Nishiyama, M. Onishi, H. Mizutani, M. Narukawa, A. Motogaito, H. Miyake, Y. Iyechika and T. Maeda, *J. Cryst. Growth*, 2000, **221**, 316-326.
41. R. Datta, M. J. Kappers, M. E. Vickers, J. S. Barnard and C. J. Humphreys, *Superlattices Microstruct.*, 2004, **36**, 393-401.

Highly-efficient GaN-based light-emitting diodes on Si (111) substrates have been achieved through the suitable reactor pressure for GaN nucleation layers growth by metal-organic chemical vapor deposition.

